Research Article

Dual-modulation difference stimulated emission depletion microscopy to suppress the background signal

Wensheng Wang,[a,†] **Chuankang Li,**[a,†] **Zhengyi Zhan,**[a] **Zhimin Zhang,**[a] **Yubing Han**[a] **Cuifang Kuang**[a,b,c,d,*] **and Xu Liu**[a,b]

[a]Zhejiang University, State Key Laboratory of Modern Optical Instrumentation, College of Optical Science and Engineering, Hangzhou, China
[b]Shanxi University, Collaborative Innovation Center of Extreme Optics, Taiyuan, China
[c]Research Center for Intelligent Chips and Devices, Zhejiang Lab, Hangzhou, China
[d]Zhejiang University, Ningbo Research Institute, Ningbo, China

Abstract. Stimulated emission depletion (STED) nanoscopy is one of the most well-developed nanoscopy techniques that can provide subdiffraction spatial resolution imaging. Here, we introduce dual-modulation difference STED microscopy (dmdSTED) to suppress the background noise in traditional STED imaging. By applying respective time-domain modulations to the two continuous-wave lasers, signals are distributed discretely in the frequency spectrum and thus are obtained through lock-in demodulation of the corresponding frequencies. The background signals can be selectively eliminated from the effective signal without compromise of temporal resolution. We used nanoparticle, fixed cell, and perovskite coating experiments, as well as theoretical demonstration, to confirm the effectiveness of this method. We highlight dmdSTED as an idea and approach with simple implementation for improving the imaging quality, which substantially enlarges the versatility of STED nanoscopy.

Keywords: super-resolution microscopy; frequency domain; background suppression; anti-Stokes excitation.

1 Introduction

Far-field fluorescence optical microscopy is an important tool for understanding the microscopic world, benefitting from its low damage to biological tissues and imaging specificity in biomedical research. However, the resolution of traditional far-field optical microscopy is limited to approximately half the wavelength owing to the diffraction limit. In the past three decades, super-resolution microscopy (or nanoscopy) was developed to break through this bottleneck.[1–4] As one of the mainstream nanoscopy techniques, stimulated emission depletion (STED) microscopy has made considerable progress and has been widely used in practical researches.[5–7] STED is typically implemented using confocal laser scanning microscopy. Apart

from the Gaussian excitation beam, STED introduces another doughnut-shaped depletion beam whose intensity profile is ideally zero in the central area and increases toward the periphery. The excitation and depletion beams should be of precise alignment in the focus volume. Through stimulated emission effect, the periphery region of the original fluorescence excited by the Gaussian excitation beam is de-excited. Hence, the fluorescence of the outer ring of the point spread function (PSF) disappears, and only fluorescence in the central area of the excitation beam is retained. Thus, the FWHM of the system PSF is compressed by the doughnut-shaped beam, and the spatial resolution is enhanced accordingly.

Practically, in addition to the background noise of the detector, there are some undesirable background signals in STED imaging, which indeed affect the spatial resolution and image quality. In general, these background signals come from two dominating sources:

---

*Address all correspondence to Cuifang Kuang, cfkuang@zju.edu.cn
†These authors contributed equally to this work.

• Fluorescence generated by the re-excitation due to the ultrahigh light doses of the depletion beam

In the STED system, the wavelength of the depletion laser is usually selected at the tail of the fluorescence emission spectrum to avoid re-excitation. However, owing to the possible limitation to the choice of depletion wavelength and the special spectral characteristics of some fluorescent samples, it would cause a relatively serious re-excitation problem and generate background signals, also called anti-Stokes excitation (AStEx).

• Residual fluorescence signal due to insufficient depletion of the inhibition beam

As mentioned above, to ensure effective depletion of the fluorescence, a high-power depletion beam is required, and the pulse width of the depletion laser pulse should be as short as possible within an appropriate range to increase the peak power. However, both of these factors cause damage to biological samples. In actual situations, sometimes the available depletion intensity is limited or a depletion laser with a relatively long pulse width is chosen, leading to an incomplete depletion of the periphery fluorescence. Thus, in actual situations, the acquired STED image consists of the effective signal in the PSF core, the nondepleted fluorescence in the PSF out-ring, and the STED-induced background, as shown in Fig. 1(d).

The past decade has witnessed the development and the high significance of background removal approaches in STED microscopy[8,9] (see Table S1 in the Supplementary Material). Those methods can be divided into three categories: time-domain, space-domain, and phasor-domain methods. As one typical representative of the time-domain technique, time-gated STED (gSTED) was developed in the earliest age, which is powerful in removing anti-Stokes background.[10–13] However, gSTED also rejects the "desired" photons, namely those that are emitted in the doughnut center.[10] Therefore, the improvement using gSTED is usually canceled out with the existence of shot noise and, furthermore, uncorrelated anti-Stokes background by continuous-wave (CW) STED excitation, which is less influenced by time-gating.[8] Since then, the double scanning technique (which belongs to space-domain method) is developed to further remove the underlying background.[14–17] Gao et al. presented the stimulated emission double depletion to remove the background signal, where the depletion pulse is divided into two successive pulses to achieve the background image containing both the excitation and depletion background signals.[15,16] Subtraction of two or more images with a specific subtracting coefficient could unveil neat background imaging. However, the acquisition speed is halved due to multiple scans, and the mismatch of images would also cause distortion.

Lock-in detection has been testified to be a feasible approach in the suppression of re-excitation fluorescence.[18] Also, dual modulation with lock-in detection has long-term compatibility to pump-probe microscopy.[19,20] To date, a phasor-domain technique, called separation of photons by lifetime tuning (SPLIT), explores analysis of lifetimes to separate fluorescence in the center of the PSF, fluorescence in the periphery of the PSF, and STED-induced background.[21–26] Sarmento et al.[22] performed dual temporal modulation of excitation and depletion beams and implemented an analysis in the phasor plot at a single frequency. Nonetheless, SPLIT is limited by shot noise, and its imaging resolution is confined.[8]

Here, we analyze with simulations and data a potentially more general situation, and a method called dual-modulation difference STED microscopy (dmdSTED) is proposed, which we classify as the frequency-domain method. The methodology of dmdSTED is to unmix space-domain signals into the frequency domain so the nondepleted fluorescence and STED-induced background are conveniently separated from the wanted fluorescent signals. The comparison of four domain techniques is provided in Table S2 in the Supplementary Material. For dmdSTED, the excitation and the depletion beams are loaded with different time-domain modulations. Thus, the time-domain characteristics of the fluorescence signal produced by the two lasers are affected by the common influence of two laser beams and reflected in the frequency domain. The signals of the different components are in accordance with the specific frequency and intensity in the spectrum. Hence, different types of signals, including the effective signal and two kinds of background signals, can be unveiled by lock-in demodulation of the corresponding frequency. Experimental calibrations based on nanoparticles, cells, and perovskite coatings have effectively validated the feasibility of this approach.

2 Materials and Methods

2.1 Theory of dmdSTED

For traditional STED [Fig. 1(a)], the excitation and depletion lasers are continuous wave or pulsed with a certain repetition frequency, so the final fluorescent signal remains the same. When the modulation of frequency f_{m1} is applied only to the excitation light, the corresponding fluorescence signal also has a frequency of f_1 [Fig. 1(b)], as published in the literature called modulated STED (mod-STED).[18]

For dmdSTED, we applied different modulation frequencies f_{m1} and f_{m2} to the excitation and depletion beams, respectively [Fig. 1(c)]. When two lasers of different frequencies are focused on the sample, via Fourier transform, the fluorescence signals with multiple frequencies are obtained. As seen from Fig. S1(b) in the Supplementary Material, the fluorescent signals are mainly distributed at four frequencies along the frequency spectrum: $f_1 - f_2$, f_1, f_2, and $f_1 + f_2$. Frequency intensity $\xi(f)$ is defined to measure the relative strength of each discrete frequency component. The spatial- and frequency-domain characteristics of different fluorescent signal components when applying dual modulation to the excitation and depletion beams are shown in Fig. 1(d). Here, "dark green" represents the fluorescence in the central area, "light green" represents the fluorescence in the outer ring area, and "yellow" represents the AStEx fluorescence in the outer ring area. The upper part of Fig. 1(d) shows that there is no AStEx, and the fluorescence in the center area only has a frequency of f_1, while the outer ring area is a combination of four frequency components at the same time. The lower part of Fig. 1(d) shows the condition in the presence of AStEx, and the fluorescence with a frequency of f_2 occurs due to re-excitation. Therefore, for actual imaging, detected fluorescence signals will present specific frequency characteristics, as shown in Fig. 1(e), where $\xi(f_1)$ contains the fluorescence in the center and outer ring area, and $\xi(f_2)$ corresponds to the fluorescence in the outer ring area, including the AStEx signal. Therefore, by demodulating a specific frequency, fluorescent signals of different components can be achieved, and then the background signal can be removed by the difference between $\xi(f_1)$ and other frequency intensities, such as $\xi(f_2)$, $\xi(f_1 - f_2)$, or $\xi(f_1 + f_2)$. Strong anti-Stokes fluorescence mainly exists at the frequency f_2. Therefore, the anti-Stokes background is removed in the demodulation stage using lock-in hardware, and
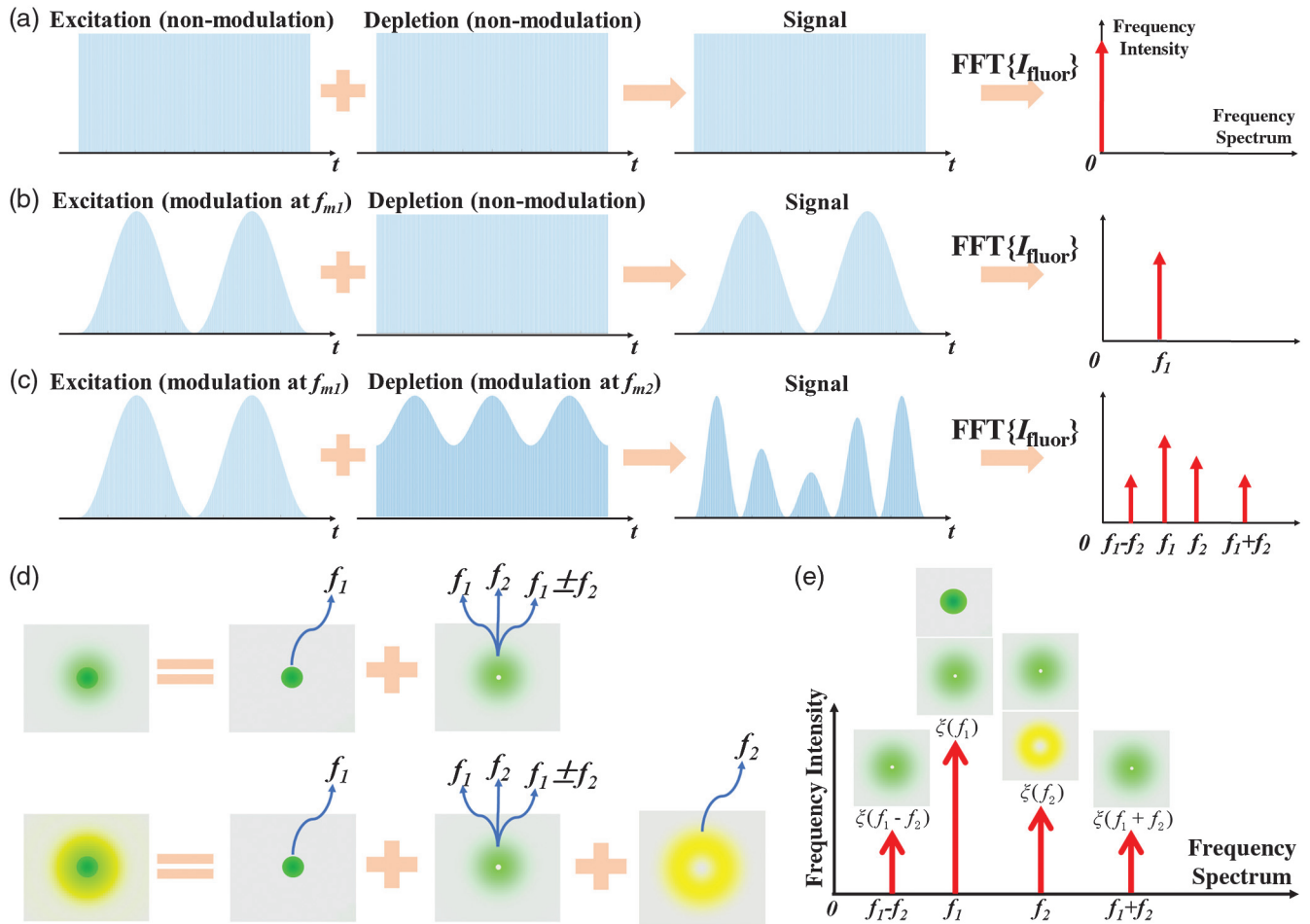
Fig. 1 Basic principle of dual-modulation difference stimulated emission depletion (dmdSTED) microscopy. (a)–(c) Time- and frequency-domain forms of the fluorescence signal and the corresponding spectrum under different modulation methods: no applied modulation, only the modulation frequency f_{m1} is applied to the excitation beam, modulation frequencies of f_{m1} and f_{m2} are simultaneously applied to the excitation and depletion beams. (d) Spatial and frequency domain characteristics of different fluorescent signal components. (e) Frequency characteristics of the finally detected fluorescence signal, where $\xi(f_1)$ contains the fluorescence in the center and outer ring areas, and $\xi(f_2)$ corresponds to the fluorescence in the outer ring area.

then the nondepleted background can be further removed through the difference between $\xi(f_1)$ and the sum frequency $\xi(f_1 + f_2)$ or the difference frequency $\xi(f_1 - f_2)$ using a carefully selected subtracting coefficient. To this end, for mod-STED, nondepleted fluorescence is mixed with the effective fluorescence at frequency f_1 in the frequency spectrum.[18] The detailed calculation of the proposed method is illustrated in Note S2 in the Supplementary Material.

Different frequency components are analyzed experimentally, as shown in Fig. 2(a). The frequency component $\xi(f_1)$ corresponds to the fluorescence in the center area and a part of the fluorescence in the outer circle. Whereas, owing to the combined effect of excitation light and depletion light with different modulation frequencies, the fluorescence in the outer ring area will contain four frequency components: $\xi(f_1)$, $\xi(f_2)$, $\xi(f_1 - f_2)$, $\xi(f_1 + f_2)$. The prominent difference between the imaging results of four frequency components is the signal intensity, as shown in Fig. 1(c). In particular, when the anti-Stokes fluorescence is not obvious, $\xi(f_2)$ can be mainly

considered as the background signal. In addition, the modulation contrast CM also has a significant effect on $\xi(f_1)$ and $\xi(f_2)$ imaging. Here, we define the modulation contrast $CM = (I_{max} - I_{min})/(I_{max} + I_{min})$, where I_{max} or I_{min} is the maximum intensity or minimum intensity of the excitation beam or depletion beam. While, CM_1 and CM_2 are the modulation contrast of the excitation and depletion beams, respectively. The influence of CM_2 is characterized by the experimental imaging in Fig. 2(b), which is also evidenced by the results in Figs. S2–S4 in the Supplementary Material. Specifically, as CM_2 increases, the signal-to-noise ratio (SNR) of $\xi(f_2)$ imaging increases, but the resolution of $\xi(f_1)$ imaging decreases accordingly [Fig. 2(b)]. Therefore, in actual imaging, the most appropriate CM_2 value should be selected considering both aspects. We also numerically and experimentally investigate the influences of either excitation beam intensity I_{exc} or depletion beam intensity I_{dep} against the signal intensities of different frequency components (see Figs. S5 and S6 in the Supplementary Material). In addition, the influence of the applied modulation
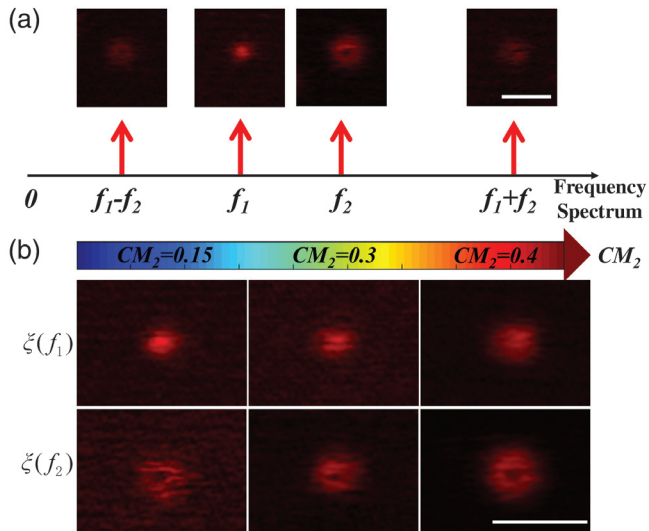
Fig. 2 Imaging analysis of fluorescence signals at different frequencies and the influence of CM_2. (a) Fluorescence signals corresponding to four frequency components. Scale bar: 400 nm. (b) Variation of $\xi(f_1)$ images and $\xi(f_2)$ images against CM_2, with values of 0.15, 0.3, and 0.4. Scale bar: 500 nm. The analysis is characterized by 40-nm fluorescent nanoparticles.

frequencies is discussed (see Figs. S7 and S8 in the Supplementary Material).

In dmdSTED, the nondepleted background can be removed through the difference between $\xi(f_1)$ and $\xi(f_1 + f_2)$ or $\xi(f_1 - f_2)$ using a subtracting coefficient, shown in the graph of Figs. S9 and S10 in the Supplementary Material. As is known, subtraction will cause negative values. The influence of the subtracting coefficient is investigated in order so that the negative value should be around 0, and we numerically demonstrate that the optimal subtracting coefficient is about 1.56 (Fig. S11 in the Supplementary Material). Numerical results on nanoparticles and microtubes show that dmdSTED affords higher discernment ability with respect to conventional STED (Figs. S12 and S13 in the Supplementary Material). Thus, given the acquired spatial resolution, dmdSTED has the potential of lower required depletion light power. The modulation transfer function (MTF) along the radial direction of the PSF is simulated. It is seen from Fig. S14 in the Supplementary Material that dmdSTED with relatively lower depletion power, such as 40 MW/cm^2, could have even larger spatial frequency in parallel to the conventional STED scenario with 100 MW/cm^2 depletion power. In our perspective, dmdSTED has the ability to reduce the applied depletion light doses, which may have the potential to alleviate the photobleaching issue. In the future, the experimental works are expected to further verify this advantage of dmdSTED. Thus, in the case of conventional STED with 100 MW/cm^2 depletion power, 40-nm spatial resolution is revealed. With our dmdSTED when $CM_2 = 0.9$, only 40 MW/cm^2 depletion power is entailed. This simulation result verifies the ability of dmdSTED in the reduction of light doses (Fig. S15 in the Supplementary Material).

The optics setup of dmdSTED is shown in Fig. S16 in the Supplementary Material. Notably, as shown in Fig. S17 in the Supplementary Material, the demodulation signal intensity is negatively correlated to the applied modulation frequency f_m.

This is limited by our acousto-optic and electro-optic modulators. Meanwhile, in the experimental setup, the time constant (TC) of the lock-in amplifier is recommended to be longer than the modulation period (T_m), which is equal to $1/f_m$.[18] In addition, the pixel dwell time T_d should be equal to or greater than TC. That is, for 100-kHz modulation, the pixel dwell time should be longer than 10 μs. Thus, if f_m is too small, T_m becomes too large, and T_d is even longer. Furthermore, a high value for T_d will induce greater noise, which results in contamination of the image quality, as well as reduced acquisition speed. We have experimentally demonstrated that the values of f_m in the range of 10 to 150 kHz are appropriate for this imaging modality, and this represents the optimal trade-off between acquisition speed and image quality. In the future, an optical modulator with even higher working frequency is highly recommended to further increase the acquisition speed and to inhibit the $1/f_m$ background noise due to laser intensity undulation.[27]

3 Results

3.1 Imaging of Nanoparticles

We tested our method using 40-nm fluorescent particles (Abberior). Practically, bias intensity is defined: $I_{\mathrm{bias}} = (I_{\max} + I_{\min})/2$. The specific experimental parameters were determined as follows: for the excitation beam, the bias intensity I_{bias} was 7 μW, CM_1 was 1, and the modulation frequency was 50 kHz; for the depletion beam, I_{bias} was 470 mW, CM_2 was 0.35, and the modulation frequency was 75 kHz. The pixel dwell time is 50 μs. Here, the choice of I_{bias} and CM_2 of the depletion beam not only guarantees the imaging resolution when the depletion intensity is at the minimum value, but also ensures that the fluorescence signal of $\xi(f_2)$ is as large as possible. Meanwhile, the depletion intensity for STED was selected at $I_{\mathrm{STED}} = I_{\mathrm{bias}} = 470$ mW, ensuring a fair comparison between STED and dmdSTED. The experimental results are presented in Fig. 3. Figures 3(a)–3(c) show the imaging results of confocal, STED, and dmdSTED. It can be seen that the resolutions of STED and dmdSTED are basically the same, but for dmdSTED the halo around the particles caused by the background signal at the periphery is relatively weakened. Signal levels are measured, and SNRs of confocal, STED, and dmdSTED are 8.96, 9.25, and 18.17, respectively. This is due to the background signal originating from the excitation beam, which can be filtered out in dmdSTED. Here, the re-excitation caused by the depletion beam is very weak owing to the selected depletion wavelength and sample. The subtracted background for dmdSTED is shown in Fig. S20(a) in the Supplementary Material. A partially enlarged view in Figs. 3(d)–3(f) and the intensity profiles in Fig. 3(g) verify the above-mentioned result in a clearer way. In both cases, the resolving ability can completely resolve 40-nm particles, and thus the FWHM values of the two profiles are almost the same. However, for STED, a part of the additional background signal is clear in the lower middle of the profile, but these signals nearly disappear in dmdSTED. Figure 3(h) shows the statistical results of the particle size distribution of the nanoparticles, with a mean value of 61 nm for dmdSTED and that of 77 nm for STED. Fourier ring correlation (FRC) analysis is also conducted, and the results show that the resolutions of confocal, STED, and dmdSTED are 211, 77, and 61 nm, respectively [Fig. S18(a) in the Supplementary Material]. A spatial transverse resolution of $\lambda/8$ is reached.
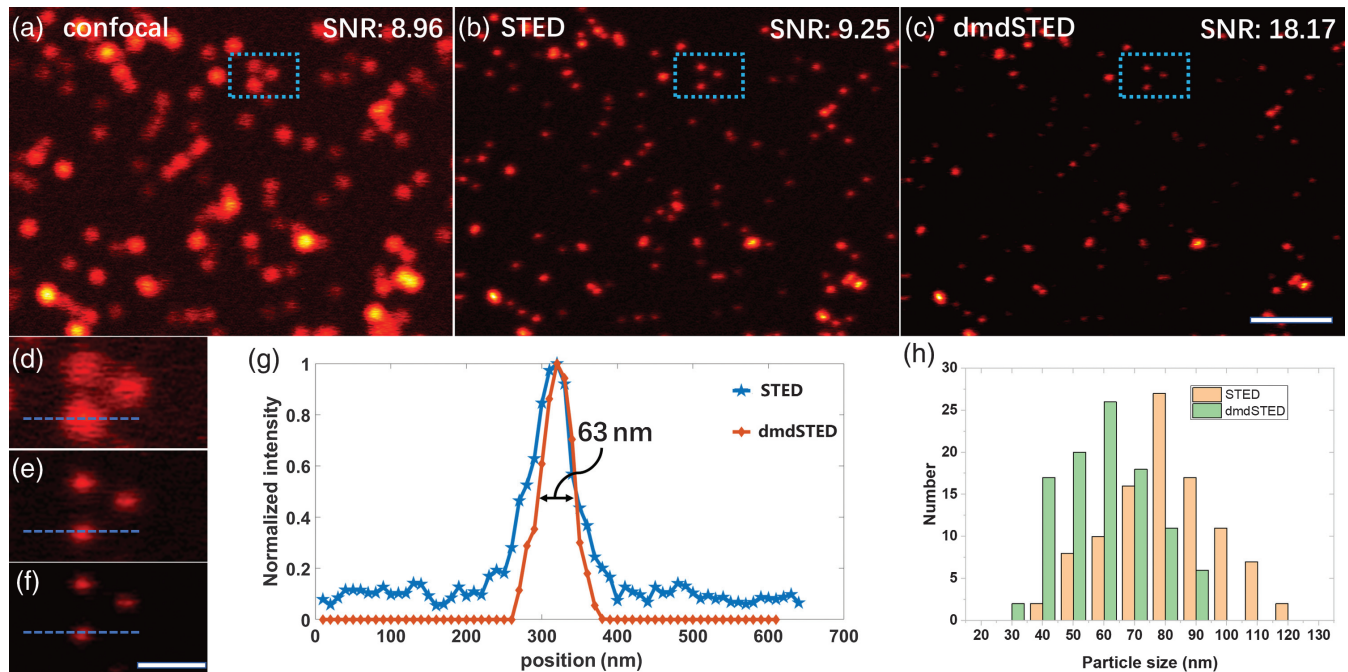
Fig. 3 40-nm particle experimental results. (a)–(c) Imaging results of confocal, STED, and dmdSTED, respectively. Scale bar: 1.5 μm. (d)–(f) Partially enlarged view of the area marked by the blue dashed box in (a)–(c). Scale bar: 300 nm. (g) Image intensity change curve at the position along the blue dotted line in (d)–(f). The blue and red lines represent STED and dmdSTED, respectively, where the FWHM of dmdSTED is 63 nm. (h) Distribution of the statistical results of the FWHM of nanoparticles.
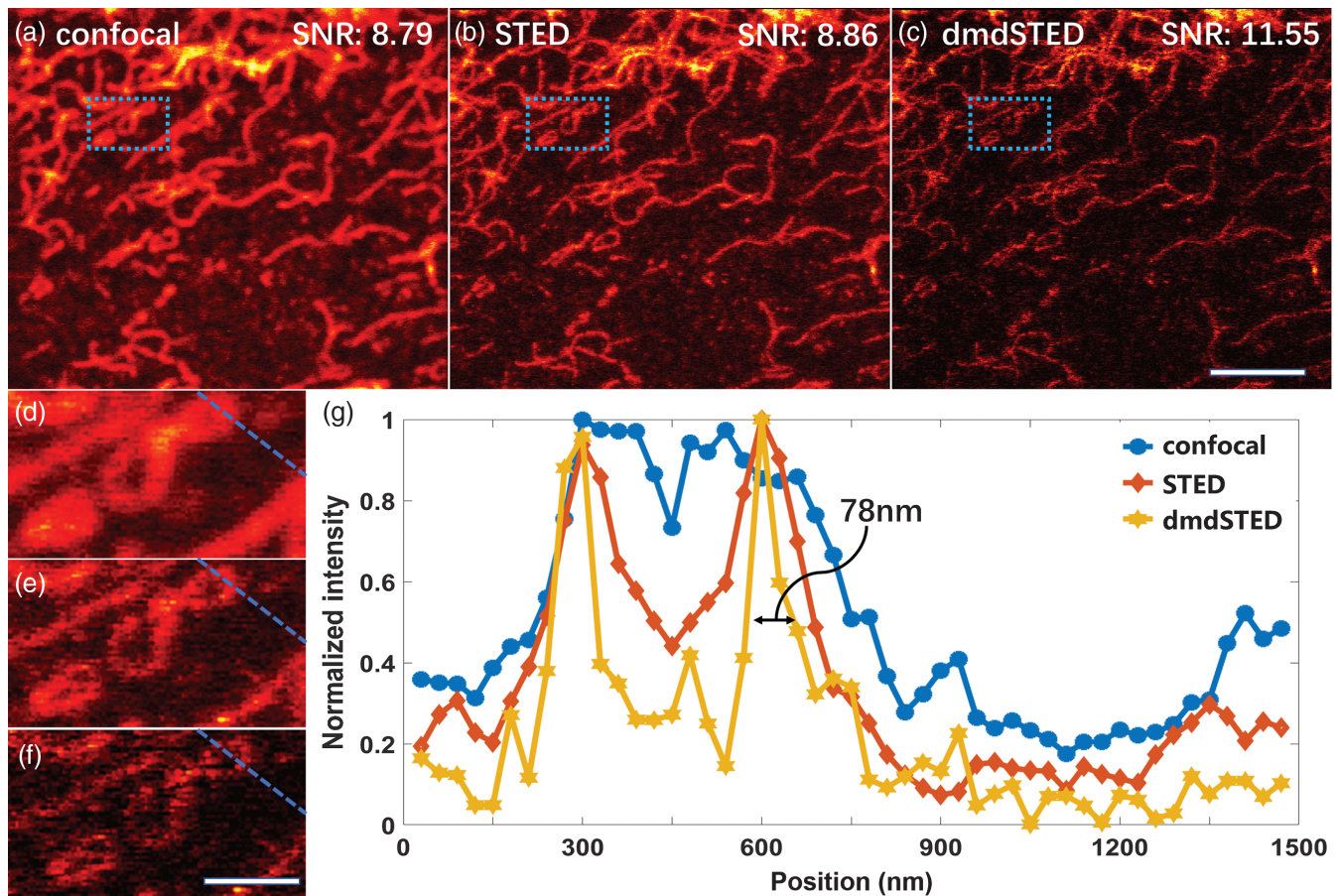
3.2 Cell Imaging of dmdSTED

Furthermore, we tested the effectiveness of the method using cell experiments. The sample was Hela cell vimentin labeled with Star Green (Abberior). The experimental parameters are generally similar to those of the nanoparticles. The CM_1 value of the excitation laser was maintained at 1, and that of the depletion laser was 0.35. The modulation frequencies of the excitation and depletion lasers were 50 and 80 kHz, respectively. Figures 4(a)–4(c) show the imaging results of confocal, STED, and dmdSTED, respectively. In order for fair comparison, the STED image is already subtracted by the optics system background (refer to Fig. S19 in the Supplementary Material). Via the demodulation at the frequency $(f_1 + f_2)$, the subtracted background for dmdSTED is shown [Fig. S20(b) in the Supplementary Material]. Also, SNRs of confocal, STED, and dmdSTED are characterized to be 8.79, 8.86, and 11.55, respectively, where 30.4% improvement of SNR is revealed in contrast to conventional STED. The results show that dmdSTED can effectively remove the undesired background in STED, and the partially enlarged images in Figs. 4(d)–4(f) show the corresponding results more clearly. We further verified the influence of CM_2 on the signal frequency intensities of the sum and difference frequencies. The experimental results are consistent with the previous theoretical analysis. Here, the most suitable CM_2 value was ∼0.5 to 0.7 (evidenced by Figs. S3 and S4 in the Supplementary Material). For a small CM_2, the desired signal strength is weakened, affecting the imaging SNR. When CM_2 is too large, the depletion intensity will decrease to a very low level, and the imaging resolution will be influenced. The results indicate that the imaging contrast and resolution can be

enhanced for a reasonable CM_2. FRC analysis is conducted, and the results show that the spatial resolutions of confocal, STED, and dmdSTED are 225, 91, and 74 nm, respectively [Fig. S18(b) in the Supplementary Material]. That is, 22.9% enhancement of spatial resolution is reached in contrast to conventional STED.

3.3 Eliminating the Anti-Stokes Background

To date, STED has been successfully applied to many samples, including organic fluorophores, fluorescent proteins, quantum dots, and color centers in diamond. However, the practical feasibility depends on the emitter's intrinsic properties of the emitter, which sometimes hampers the applicability of STED imaging. Organometallic halide perovskites are attracting considerable research interest as a promising candidate for next generation solar cells. Currently, the dominant observation method for this material is scanning electron microscopy. The as-published literature has reported the successful utilization of STED on CsPbBr$_3$ quantum dots.[28] In this study, we attempted to observe perovskite using our optical system. A remarkable feature of perovskite is its high fluorescence brightness, including anti-Stokes fluorescence. Hence, we introduce it to the experiments here to verify our method for removing anti-Stokes fluorescence noise.

Figures 5(a)–5(c) show the confocal, STED, and dmdSTED images, respectively. For the STED modality, the perovskite exhibits strong absorption of the depletion light and produces strong anti-Stokes fluorescence, exhibited in Fig. 5(d), which is even stronger than the effective fluorescence and severely hinders the application of STED imaging on this material.

Fig. 4 Biological cell imaging results. The imaging results of (a) confocal, (b) STED, and (c) dmdSTED. Scale bar: 2 μm. (d)–(f) Partially enlarged view of parts indicated by the blue dashed box in (a)–(c). Scale bar: 1 μm. (g) Image intensity variation curve along the blue dotted line. The blue, red, and yellow lines correspond to confocal, STED, and dmdSTED, respectively. The sample used here is vimentin labeled with Star Green.

Figure 5(e) shows the respective intensities of confocal, STED, dmdSTED, and anti-Stokes fluorescence, which indicates that the anti-Stokes background is comparable to the confocal image. For the reason that the normalized intensities of the four images are similar and the subdiffraction effect of the perovskite is not obvious, it is caused by two aspects. First, an obvious feature of perovskite is its high fluorescence brightness, which can emit strong fluorescence under extremely weak excitation light intensity (here we employ 1-μW I_{exc}, which is 1/10 of the applied excitation power for common fluorescent samples). Hence, it also shows decent brightness in the dmdSTED condition. Second, because of the large size of the sample used here, perovskites are agglomerated possibly in the order of hundreds of nanometers. Thus, the fluorescence signal intensity is further enhanced. Therefore, the signal intensity decline of dmdSTED is limited in Fig. 5(e). In addition, the anti-Stokes fluorescence exhibited fluorescence intensity close to that of confocal, but the STED intensity was slightly lower than the two, which we believe is mainly due to the relatively higher photobleaching in STED, resulting in a decrease of the mean intensity of STED imaging.

By demodulating at the specific frequency f_2, the anti-Stokes fluorescence can be effectively filtered. Here, the nondepletion background signal was obtained by demodulating the frequencies $f_1 \pm f_2$, which is also the subtracted background, as shown in Fig. S20(c) in the Supplementary Material, where hollow features in some areas are presented. This phenomenon confirms to a certain extent that the solid and hollow beams work at the same time, and the stimulated emission effect indeed occurs. The FWHM with the line plot is 273 nm with dmdSTED imaging, as shown in Fig. 5(f), achieving the imaging of the perovskite coating. FRC analysis is conducted, and the results show that the spatial resolutions of confocal, STED, and dmdSTED are 320, 241, and 205 nm, respectively [Fig. S18(c) in the Supplementary Material]. To this end, dmdSTED can effectively separate different types of signals and enhance the imaging resolution.

4 Discussion and Conclusion

In this study, a STED method was proposed combined with temporal double modulation (dmdSTED) that we term the frequency-domain background suppression method. The conspicuous novelty of STED is to discriminate molecules via fluorescent on- and off-switching in the energy level regime, circumventing the spatial diffraction limit in conventional microscopies. In a like manner, dmdSTED discriminates detected signals in the frequency spectrum, which are difficult
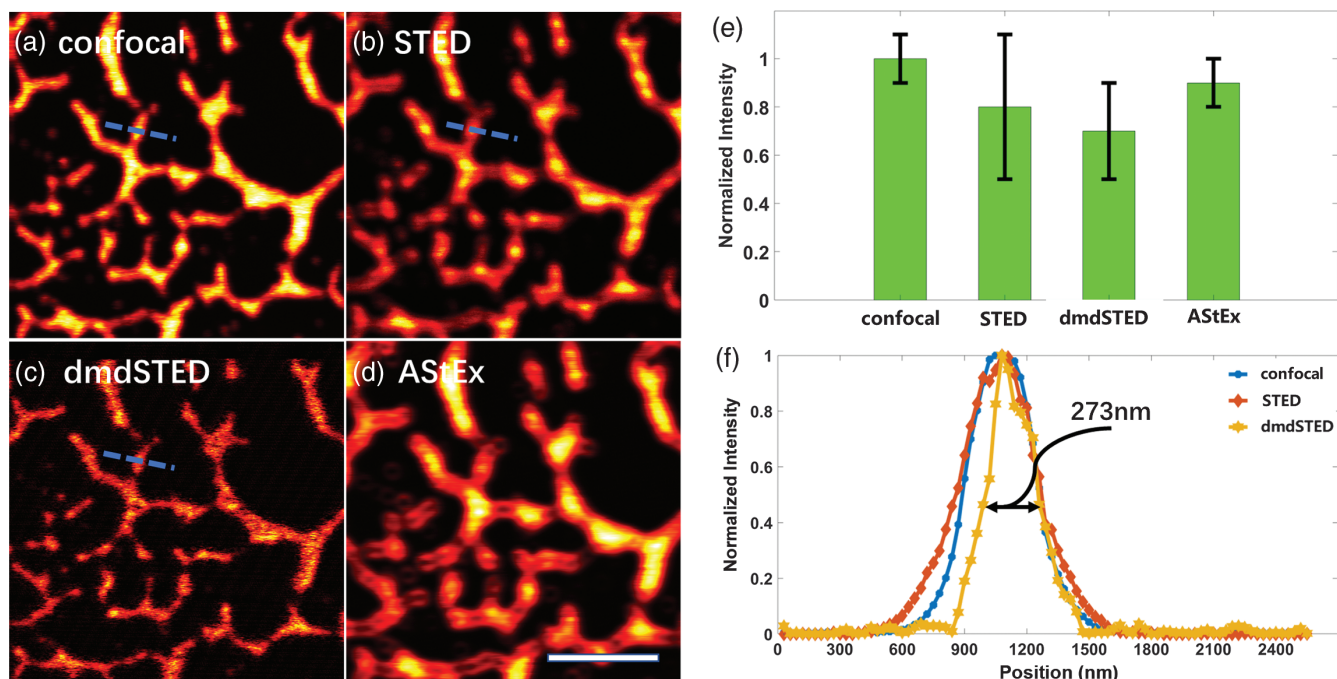
Fig. 5 Imaging of perovskite coating. Imaging results of (a) confocal, (b) STED, and (c) dmdSTED. (d) Anti-Stokes fluorescence through demodulating the frequency f_2. (e) Signal intensity bars of confocal, STED, dmdSTED, and anti-Stokes fluorescence. (f) Intensity profiles along the blue dashed lines in (a)–(c). Scale bar: 2.5 μm.

to tell apart in the space- or time-domain. We validate that the current version of dmdSTED has spatial resolution of $\lambda/8$, which is higher than that of phasor-domain method (such as SPLIT, $\lambda/5$) that is prone to being affected by shot noise. Theoretically, potential signal loss by time-domain approaches (such as time-gating) can be avoided by our approach. In addition, dmdSTED is compatible for either the pulsed or CW scenario, and hardware such as time-correlated single-photon counting is not required. Compared with the space-domain method, time resolution of dmdSTED is not confined. Thus, dmdSTED is advantageous in the acquisition of comprehensively fine images, in either spatial resolution, SNR, or time resolution. This frequency-domain method possesses the high potential to integrate into other dual-beam point-scanning techniques, such as excited state saturation microscopy,[29] charge state depletion microscopy,[30] and ground state depletion microscopy.[31]

However, the current version of the dmdSTED system is limited by its acquisition speed due to hardware. In our future study, a high frequency modulation device (above ~1 MHz) will be employed so real-time imaging for living cells becomes possible. Furthermore, by accommodating the modulation contrast, the applied depletion beam power can be lowered by 60% so the bleaching problem is alleviated. This framework has been numerically validated (Fig. S15 in the Supplementary Material), and the related experimental work is highly expected in further study. Benefitting from avoiding the re-excitation caused by the depletion beam, a depletion laser with a wavelength closer to the peak of the fluorescence emission spectrum of the sample can be selected, thus reducing the required depletion intensity. In addition, it can accept more types of samples with spectral characteristics different from commonly used fluorescent dyes

in STED, such as some quantum dots with a wider excitation spectrum.[10,12,14]

References

1. S. W. Hell, "Far-field optical nanoscopy," *Science* **316**(5828), 1153–1158 (2007).
2. R. Heintzmann and M. G. Gustafsson, "Subdiffraction resolution in continuous samples," *Nat. Photonics* **3**(7), 362–364 (2009).
3. M. J. Rust, M. Bates, and X. Zhuang, "Sub-diffraction-limit imaging by stochastic optical reconstruction microscopy (STORM)," *Nat. Methods* **3**(10), 793–796 (2006).
4. E. Betzig et al., "Imaging intracellular fluorescent proteins at nanometer resolution," *Science* **313**(5793), 1642–1645 (2006).
5. F. Bottanelli et al., "Two-colour live-cell nanoscale imaging of intracellular targets," *Nat. Commun.* **7**, 10778 (2016).

6. J. Chojnacki et al., "Envelope glycoprotein mobility on HIV-1 particles depends on the virus maturation state," *Nat. Commun.* **8**, 545 (2017).
7. W. Shin et al., "Visualization of membrane pore in live cells reveals a dynamic-pore theory governing fusion and endocytosis," *Cell* **173**(4), 934–945.e12 (2018).
8. Y. Ma and T. Ha, "Fight against background noise in stimulated emission depletion nanoscopy," *Phys. Biol.* **16**(5), 051002 (2019).
9. C. Li et al., "Resolution enhancement and background suppression in optical super-resolution imaging for biological applications," *Laser Photonics Rev.* **15**(1), 1900084 (2020).
10. G. Vicidomini et al., "STED with wavelengths closer to the emission maximum," *Opt. Express* **20**(5), 5225–5236 (2012).
11. I. C. Hernandez et al., "A new filtering technique for removing anti-Stokes emission background in gated CW-STED microscopy," *J. Biophotonics* **7**(6), 376–380 (2014).
12. M. D. Bordenave et al., "STED nanoscopy with wavelengths at the emission maximum," *J. Phys. D Appl. Phys.* **49**(36), 365102 (2016).
13. M. Castello et al., "Removal of anti-Stokes emission background in STED microscopy by FPGA-based synchronous detection," *Rev. Sci. Instrum.* **88**(5), 053701 (2017).
14. J. Hanne et al., "STED nanoscopy with fluorescent quantum dots," *Nat. Commun.* **6**, 7127 (2015).
15. P. Gao et al., "Background suppression in fluorescence nanoscopy with stimulated emission double depletion," *Nat. Photonics* **11**(3), 163–169 (2017).
16. P. Gao and G. U. Nienhaus, "Precise background subtraction in stimulated emission double depletion nanoscopy," *Opt. Lett.* **42**(4), 831–834 (2017).
17. J. C. Lee et al., "Accurate background subtraction in STED nanoscopy by polarization switching," *ACS Photonics* **6**(7), 1789–1797 (2019).
18. E. Ronzitti, B. Harke, and A. Diaspro, "Frequency dependent detection in a STED microscope using modulated excitation light," *Opt. Express* **21**(1), 210–219 (2013).
19. C. Y. Fan et al., "All-optical fluorescence image recovery using modulated stimulated emission depletion," *Chem. Sci.* **2**(6), 1080–1085 (2011).
20. S. Das et al., "Background free imaging in stimulated emission fluorescence microscopy," *J. Opt.* **21**(12), 125301 (2019).
21. L. Lanzano et al., "Encoding and decoding spatio-temporal information for super-resolution microscopy," *Nat. Commun.* **6**, 6701 (2015).
22. M. J. Sarmento et al., "Exploiting the tunability of stimulated emission depletion microscopy for super-resolution imaging of nuclear structures," *Nat. Commun.* **9**, 3415 (2018).
23. L. Wang et al., "Resolution improvement in STED super-resolution microscopy at low power using a phasor plot approach," *Nanoscale* **10**(34), 16252–16260 (2018).
24. G. Tortarolo et al., "Photon-separation to enhance the spatial resolution of pulsed STED microscopy," *Nanoscale* **11**(4), 1754–1761 (2019).
25. Y. Chen et al., "Elimination of re-excitation in stimulated emission depletion nanoscopy based on photon extraction in a phasor plot," *Laser Photonics Rev.* **14**(3), 1900352 (2020).
26. S. Pelicci et al., "Improving SPLIT-STED super-resolution imaging with tunable depletion and excitation power," *J. Phys. D Appl. Phys.* **53**(23), 234003 (2020).
27. W. Min et al., "Coherent nonlinear optical imaging: beyond fluorescence microscopy," *Annu. Rev. Phys. Chem.* **62**(1), 507–530 (2011).
28. S. Ye et al., "Low-saturation-intensity, high-photostability, and high-resolution STED nanoscopy assisted by $CsPbBr_3$ quantum dots," *Adv. Mater.* **30**(23), 1800167 (2018).
29. B. Yang et al., "Optical nanoscopy with excited state saturation at liquid helium temperatures," *Nat. Photonics* **9**(10), 658–662 (2016).
30. X. D. Chen et al., "Subdiffraction optical manipulation of the charge state of nitrogen vacancy center in diamond," *Light-Sci. Appl.* **4**, e230 (2015).
31. K. Y. Han et al., "Metastable dark states enable ground state depletion microscopy of nitrogen vacancy centers in diamond with diffraction-unlimited resolution," *Nano Lett.* **10**(8), 3199–3203 (2010).
32. C. Eggeling, A. Volkmer, and C. A. Seidel, "Molecular photobleaching kinetics of rhodamine 6G by one- and two-photon induced confocal fluorescence microscopy," *ChemPhysChem* **6**(5), 791–804 (2005).
33. C. Ringemann et al., "Enhancing fluorescence brightness: effect of reverse intersystem crossing studied by fluorescence fluctuation spectroscopy," *ChemPhysChem* **9**(4), 612–624 (2008).

Wensheng Wang is a PhD candidate in the College of Optical Science and Engineering at Zhejiang University in Hangzhou, Zhejiang. His research fields are fluorescent super-resolution microscopy and pump-probe imaging.

Chuankang Li received his PhD in the College of Optical Science and Engineering at Zhejiang University in Hangzhou, Zhejiang, in 2021. Recently, he is a postdoc in the College of Optical Science and Engineering at Zhejiang University. His research fields are fluorescent point-scanning super-resolution microscopy, inorganic fluorescent labels, and single-molecular localization imaging.

Cuifang Kuang received his PhD in the School of Science at Beijing Jiaotong University in 2007. From June of 2007 to January of 2008, he was a postdoctoral researcher at Beijing Institute of Technology. From February of 2008 to February of 2010, he was a postdoctoral researcher in the Department of Mechanical Engineering at the University of South Carolina. From September of 2014 to September of 2015, he was a visiting scholar at Massachusetts Institute of Technology. Now, he is a professor at Zhejiang University in the College of Optical Science and Engineering, with research interests in optical super-resolution imaging and photolithography.

Biographies of the other authors are not available.